JOURNAL OF MATERIALS SCIENCE 28 (1993) 3923–3930

Interfacial debonding and fibre pull-out stresses

Part III *Interfacial properties of cement matrix composites*

JANG-KYO KIM, LI-MIN ZHOU, YIU-WING MAI
Centre for Advanced Materials Technology, Department of Mechanical Engineering, University of Sydney, Sydney, New South Wales 2006, Australia

Following the development of an improved theoretical analysis of fibre pull-out on the basis of the concept of fracture mechanics in Part II of this paper, the theory has been successfully used to characterize the debonding and frictional pull-out behaviour in cement mortar matrix composites reinforced with steel and glass fibres. It is shown from the plots of partial debond stress, σ_d^p, versus debond length, ℓ, that these composites are typical of mechanical bonds at the interface. For the steel fibre–cement matrix composites, the theory overestimates the post-debond frictional pull-out stress, σ_{fr}, particularly for long embedded fibre length, L, otherwise the prediction agrees well with the experiments for the maximum debond stress, σ_d^*. This seems to be a direct result of decay of frictional bonds at the interface region after debonding due mainly to compaction of the porous cement mortar surrounding the fibre, effectively reducing the residual clamping stress, q_0, arising from shrinkage of the cement matrix. Therefore, a correct theoretical prediction is made for σ_{fr} using a lower value of q_0 while other parameters are kept constant, which gives good agreement with experimental results. For glass fibre–cement matrix composites, an accelerated cure condition promotes rapid hydration of cement and densification of the matrix. This effectively improves the chemical as well as mechanical bonds at the fibre–matrix interface through the formation of CH crystals and large fibre–solid matrix contact area of the interface, and consequently ameliorating the interfacial properties, interfacial fracture toughness, G_{ic} and q_0 in particular. Predictions of σ_d^* and σ_{fr} taking into account these changes due to cure condition, results in good agreement with experimental results.

1. Introduction

The efficient design and appropriate use of fibre composites requires a fundamental understanding of how the fracture process initiates and progresses to final failure. In particular, the interface-related failure mechanisms play a decisive role in determining gross structural integrity and damage tolerance of the composite. The recognition of the importance of the interfacial properties has led to an increased effort in both micromechanical and experimental characterization of the fibre–matrix interface in various loading configurations, including fibre pull-out, as discussed in a recent review by the authors [1]. There are two distinct approaches to the theoretical analysis of fibre pull-out: one is based on a maximum shear stress criterion such that debonding occurs when the interfacial shear stress exceeds the shear bond strength, τ_b; and the other based on the concept of fracture mechanics where the debonded region is considered as an interfacial crack and its propagation is dependent on the energy balance in terms of interfacial fracture toughness G_{ic}. In Part II of this paper [2] an improved analysis was developed on the basis of the concept of fracture mechanics, in which the differential total elastic energy stored in the composite constituents at both bonded and debonded regions are equated to the interfacial fracture toughness. Poisson contraction of the fibre when subjected to tension is considered, which results in a generalized non-uniform friction along the debonded region. The interfacial properties were determined by evaluating experimental results with regard to fibre pull-out parameters in a procedure proposed in Part I of this paper [3]. Excellent agreement was obtained for the maximum debond stress, σ_d^*, and the initial frictional pull-out stress, σ_{fr}, after complete debonding between theories and fibre pull-out experiments of several composite systems with epoxy and ceramic matrices.

The principal aim of the present study was to characterize properly the interfacial properties of cement mortar matrix composites by comparing the theory with published fibre pull-out experimental data, and thus the applicability of the theory to these composites is examined. Causes of any anomaly observed in the fibre pull-out experiments of these materials are clarified in terms of the relationship between microstructure and failure mechanisms at the fibre–matrix interface region, and their effects are correctly reflected for the interfacial properties. Further, any differences in the interfacial properties arising from different curing conditions are identified, and their implications on the fibre pull-out parameters are discussed. Ultimately,

following the successful application of the improved fibre pull-out model to several epoxy and ceramic matrix composites in Part II of this paper [2], it is intended to prove here that the model, in general, can be applied to characterize the interfacial properties of brittle fibre–brittle matrix composites, regardless of the nature of the bonding at the interface.

2. Theory

This section summarizes the interfacial debond and fibre pull-out model developed in Part II of this paper [2]. A simple shear-lag model shown in Fig. 1 consists of a fibre (of radius a) which is embedded at the centre of a coaxial cylindrical shell of matrix (of an outer radius b). L is the total embedded fibre length with a partial debonded region ℓ from the free fibre-end. The matrix is fixed at one end ($z = L$) and a tensile stress, σ, is applied to the other end ($z = 0$) of the embedded fibre. Shear-lag analyses for other boundary conditions including restrained matrix top, and fixed matrix and fibre bottom ends are given elsewhere [4]. The external stress, σ, is represented by σ_0, σ_d^p, σ_d^* and σ_{fr} for frictionless (initial) debond stress, partial debond stress, maximum debond stress and initial frictional pull-out stress after complete debonding, respectively, at different stages of the fibre pull-out process. The solution for the partial debond stress during progressive debonding was formulated as a function of the debond length, ℓ, and the crack-tip debond stress, σ_l, which is the fibre axial stress acting at the boundary between bonded and debonded region ($z = \ell$)

$$\sigma_d^p = \sigma_\ell + (\bar{\sigma} - \sigma_\ell)\frac{\omega[\exp(\lambda\ell) - 1]}{1 + \omega[\exp(\lambda\ell) - 1]} \approx \sigma_\ell + (\bar{\sigma} - \sigma_\ell)[1 - \exp(-\lambda\ell)] \quad (1)$$

Therefore, using Equation 1 the initial debond stress, σ_0, can be determined for an infinitesimal debond length (i.e. $\ell \to 0$) and the maximum debond stress, σ_d^*, determined at load instability [5]. Further, the solution for the initial frictional pull-out stress, σ_{fr}, after complete debonding is obtained when the debond length, ℓ, reaches the embedded length, L, and $\sigma_\ell = 0$

$$\sigma_{fr} = \frac{\omega\bar{\sigma}[\exp(\lambda L) - 1]}{1 + \omega[\exp(\lambda L) - 1]} \approx \bar{\sigma}[1 - \exp(-\lambda L)] \quad (2)$$

λ is the reciprocal length giving the effective friction shear stress transfer distance and $\bar{\sigma}$ is the asymptotic debond stress for long embedded length, L. These parameters are related, respectively, to the coefficient of friction, μ, and the residual clamping stress, q_0 (caused by the matrix shrinkage and differential thermal contraction between fibre and matrix) by

$$\lambda = \frac{2\mu k}{a} \quad (3)$$

$$\bar{\sigma} = -\frac{q_0}{k}[1 + (\gamma/\alpha)(\nu_m/\nu_f)] \quad (4)$$

where $\alpha = E_m/E_f$ (Young's modulus ratio of the matrix to the fibre), $k = (\alpha\nu_f + \gamma\nu_m)/[\alpha(1 - \nu_f) + 1 + \nu_m + 2\gamma]$, $\gamma = a^2/(b^2 - a^2)$ (fibre volume ratio to the matrix) and $\omega = \alpha\nu_f/(\alpha\nu_f + \gamma\nu_m)$. ν_f and ν_m are the fibre and matrix Poisson's ratios. The partial debond stress, σ_d^p, in Equation 1 is composed of two components: (i) a crack-tip debond stress, σ_ℓ, which is a function of the interfacial fracture toughness, G_{ic}, and the debond length, ℓ, relative to L; (ii) a friction stress component which is directly proportional to $(\bar{\sigma} - \sigma_\ell)$ and is also a function of λ.

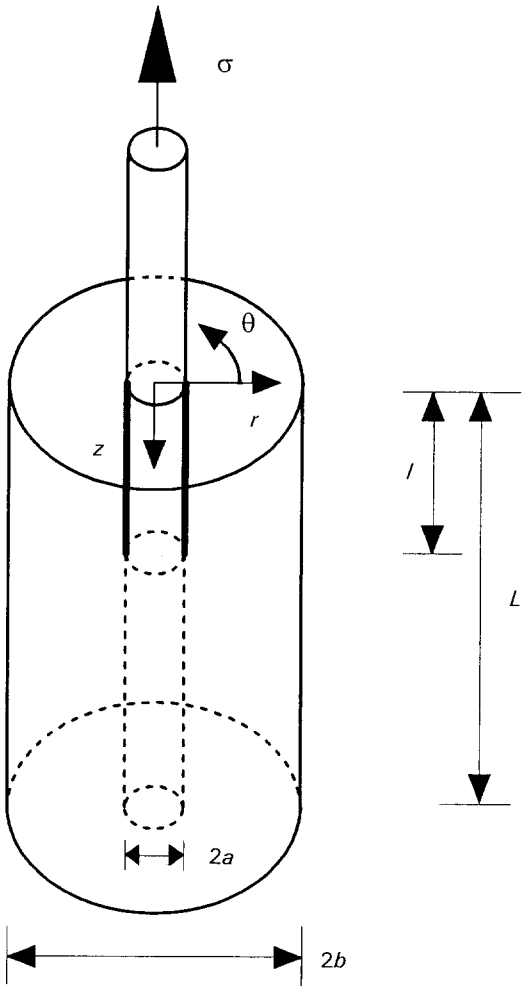

Figure 1 A schematic illustration of the fibre pull-out model.

3. Results

3.1. Fibre pull-out experiments

Published fibre pull-out experimental data for cement mortar (or paste) matrix composites with two different reinforcements, namely steel and glass fibres, are compared with theoretical predictions. Only those [6–11] with both the maximum debond stress, σ_d^*, and the post-debond frictional pull-out stress, σ_{fr}, available (or at least can be derived from the information provided if not directly measured) were selected. This is necessary to determine the fibre pull-out parameters σ_0, λ and $\bar{\sigma}$ (and thus the interfacial properties G_{ic}, μ and q_0) simultaneously using the theory described in Section 2. To avoid any complications arising from experimental variations within a given data group taken from different sources, particularly the elastic

TABLE I Fibre pull-out experimental conditions

Reference	Fibre			Matrix	
	Material	Effective fibre radius, a (mm)	Embedded fibre length, L (mm)	Mixture ratio by weight (sand : cement : water)	Effective matrix radius, b (mm)
Naaman and Shah [6]	Music wire and brass-coated steel wire	0.076–0.2	12.7	(2.5 : 1 : 0.55) cured for 7–9 days	12.7 max.
Maage [7]	Steel wire	0.19	9.2–15.8	(3 : 1 : 0.5) cured for 28 days	11 max.
Beaumont and Aleszka [8]	Brass-coated steel wire	0.25	6–31	(2.3 : 1 : 0.3) cured for 28 days and overnight dry at 105 °C	5.0
Gray [9]	Brass-coated steel wire	0.19	25–125	(3 : 1 : 0.5) cured in water for 28 days	12.7
Mandel *et al.* [10]	Steel wire	0.25	20	(1.5 : 1 : 0.43)	6.4 max.
Li *et al.* [11]	Alkali-resistant glass fibre	0.09	3–21	(?: 1 : 0.35) cured for 3 days in air or in lime-saturated water at 50 °C	7.15

TABLE II Representative values for elastic properties and effective radii of constituents

Composite system	Elastic properties				Effective radii	
	E_f (GPa)	E_m(GPa)	ν_f	ν_m	a (mm)	b (mm)
Steel wire–cement matrix	207	30.4	0.27	0.17	0.19	12.7
Glass fibre–cement matrix	72.0	30.4	0.22	0.17	0.09	7.15

properties and radii of the fibre and matrix, only those data for composites with similar properties are chosen for evaluation. The details of experimental conditions for the fibre pull-out results and the representative properties for each data group used for prediction in the present study are summarized in Tables I and II, respectively. For steel fibre–cement matrix composites, data were taken from five different sources and the elastic properties given in Table II were taken from the work of Gray [9] who measured the maximum debond stress, σ_d^*, and post-debond frictional stress, σ_{fr}, for a wide range of embedded fibre length, L. For glass fibre–cement matrix composites, a large amount of information is available for the interfacial properties, mainly the interfacial shear bond strength, τ_b, determined from σ_d^* for a given embedded fibre length, L. See, for example, Bartos [12] and Proctor *et al.* [13] for reviews on this topic, and de Vekey and Majumdar [14, 15] and Laws *et al.* [16] for some experimental data. However, data for σ_{fr} are scarcely reported, probably due to the lack of clear-cut load drop at instability in the pull-out force versus displacement curve, particularly when multiple fibres are used in pull-out experiments as is the normal case for this composite system. Therefore, the initial frictional pull-out stresses, σ_{fr}, after maximum load were calculated based on the data [11] of frictional shear force per unit length for different embedded fibre lengths. Li *et al.* [11] determined the frictional shear force by using a bundle of 204 individual fibres of radius 6 μm in multiple fibre pull-out experiments. For simplicity, the bundle fibre was regarded as a single fibre of approximately 90 μm in effective radius, calculated based on the cross-sectional area of the equivalent bundle for maximum packing density in hexagonal packing (= 0.907 [17]).

The interfacial properties are determined by evaluating experimental results with regard to σ_0, λ and $\bar{\sigma}$ in a procedure similar to that presented in Part I of this paper [3], and are summarized in Table III. Using these interfacial properties (including the uncorrected values $\bar{\sigma} = 1.62$ GPa or $q_0 = -50.3$ MPa for the steel fibre composite), and the properties given in Table II, theoretical results of the partial debond stress, σ_d^p, are calculated against debond length, ℓ for different embedded fibre lengths as shown in Figs 2 and 3 for steel fibre- and glass fibre–cement matrix composites, respectively. The maximum debond stress, σ_d^*, and the initial frictional pull-out stress, σ_{fr}, are calculated based on the stresses just before and after load instability, respectively, in σ_d^p versus ℓ curves (shown in Figs 2 and 3), and are compared with experimental results in Figs 4 and 5 for steel fibre- and glass fibre–cement mortar matrix composites, respectively. The interfacial shear bond strength, τ_b, and the frictional shear strength, τ_f, given in Table III are determined using a fibre pull-out model [18, 19] developed based on the shear strength criterion as in Part I of this paper [3]

$$\tau_b = \frac{a}{2(1 + \gamma/\alpha)} \left[\frac{d\sigma_d^*}{dL} \right]_{L \to 0} \quad (5)$$

and, similarly

$$\tau_f = \frac{a}{2(1 + \gamma/\alpha)} \left[\frac{d\sigma_{fr}}{dL} \right]_{L \to 0} \quad (6)$$

TABLE III Interfacial properties for cement mortar matrix composites

Composite system	Cure condition	Fibre pull-out parameters				Interfacial properties				
		σ_0 (GPa)	λ (mm^{-1})	$\bar{\sigma}$ (GPa)	z_{max} (mm)	G_{ic} ($J m^{-2}$)	μ	q_0 (MPa)	τ_b (MPa)	τ_f (MPa)
Steel fibre-cement matrix	See Table I	0.106	0.0269	0.78 (1.62)[a]	1.2	2.50	0.082	− 24.2 (− 50.3)[a]	8.47	1.95 (4.07)[a]
Glass fibre–cement matrix	Normal cure	0.01	0.193	0.325	0.14	0.03	0.14	− 20.14	2.95	2.73
	Accelerated cure	0.274	0.138	0.545	0.64	22.82	0.10	− 33.8	40.0	3.33

[a] uncorrected values.

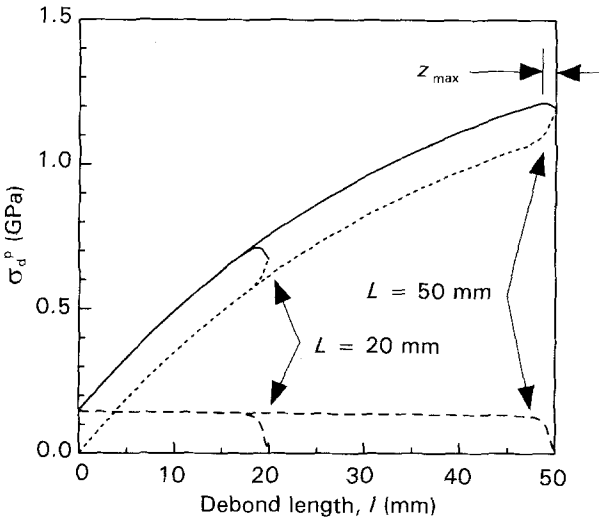

Figure 2 Plots of partial debond stress, σ_d^p, as a function of debond length, ℓ, for steel fibre–cement mortar matrix composites. (——) Partial debond stress, σ_d^p; (– – –) crack-tip debond stress, σ_l; (---) friction stress component.

where the differential terms $[d\sigma_d^*/dL]_{L\to 0}$ and $[d\sigma_{fr}/dL]_{L\to 0}$ are taken from the initial slope of the σ_d^* versus L and σ_{fr} versus L curves, respectively. Therefore, they represent a maximum value for a very short embedded fibre length, L. It is noted that τ_f values given in Table III are almost identical to those calculated based on the simple relation $\tau_{f(max)} \approx -\mu q_0$ when neglecting the Poisson contraction effect.

3.2. Steel fibre–cement mortar matrix composites

Fig. 2 clearly shows that the cement matrix composite is typical of frictional bonding at the fibre–matrix interface as evinced by the major contribution of the friction stress component to the partial debond stress, σ_d^p (i.e. over 80% at instability for L = 50 mm). This is further manifested by the very small z_{max} (= 1.2 mm) which is the maximum bond length for unstable debonding. The instability condition described in the authors' previous paper [5] requires that the derivative of σ_d^p with respect to the remaining bond length $(L - \ell)$ is equal to or less than zero. This implies that the debond process becomes unstable if L or $(L - \ell)$ is smaller than z_{max} where the maximum debond stress, σ_d^*, is obtained. It is predicted that a two-fold increase in the interfacial fracture toughness, G_{ic} (and thus a corresponding increase in the frictionless initial debond stress, σ_0, from 0.106 GPa to 0.15 GPa), would result in only a negligible increase in the partial debond stress, σ_d^p. This further implies that the chemical bond (which is represented either by the interfacial fracture toughness, G_{ic}, or shear bond strength, τ_b) makes up only an insignificant contribution to the total bond quality at the interface of this material while the frictional bond (which is a function of the residual clamping stress, q_0, and the coefficient of friction, μ) is a predominant source for the interfacial bond strength in this composite material.

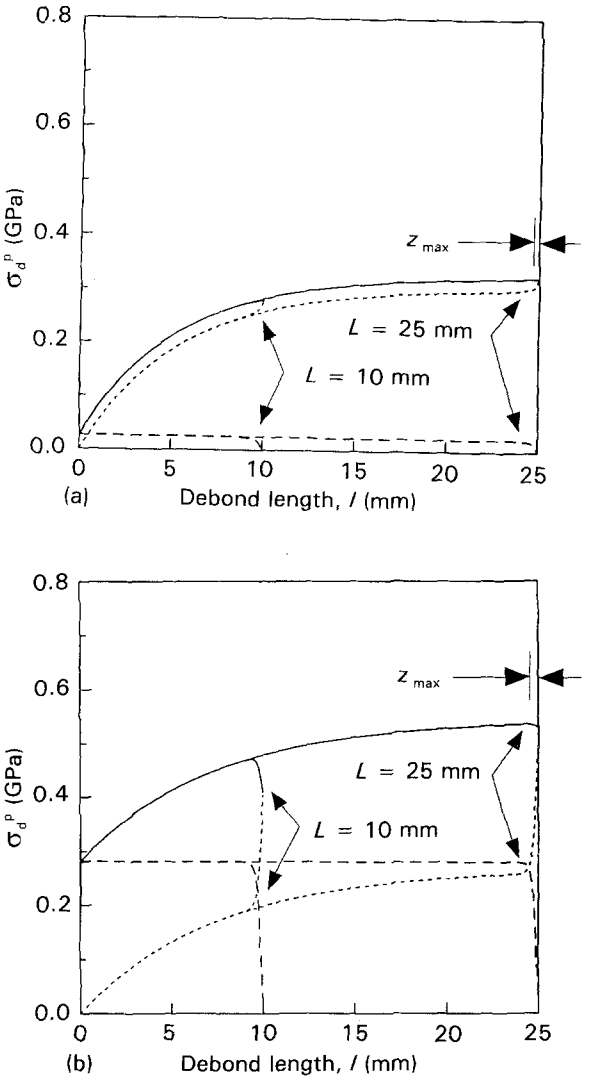

Figure 3 Plots of partial debond stress, σ_d^p, as a function of debond length, ℓ, for glass fibre–cement mortar matrix composites with (a) normal cure and (b) accelerated cure: (——) Partial debond stress, σ_d^p; (– – –) crack-tip debond stress, σ_l; (---) friction stress component.

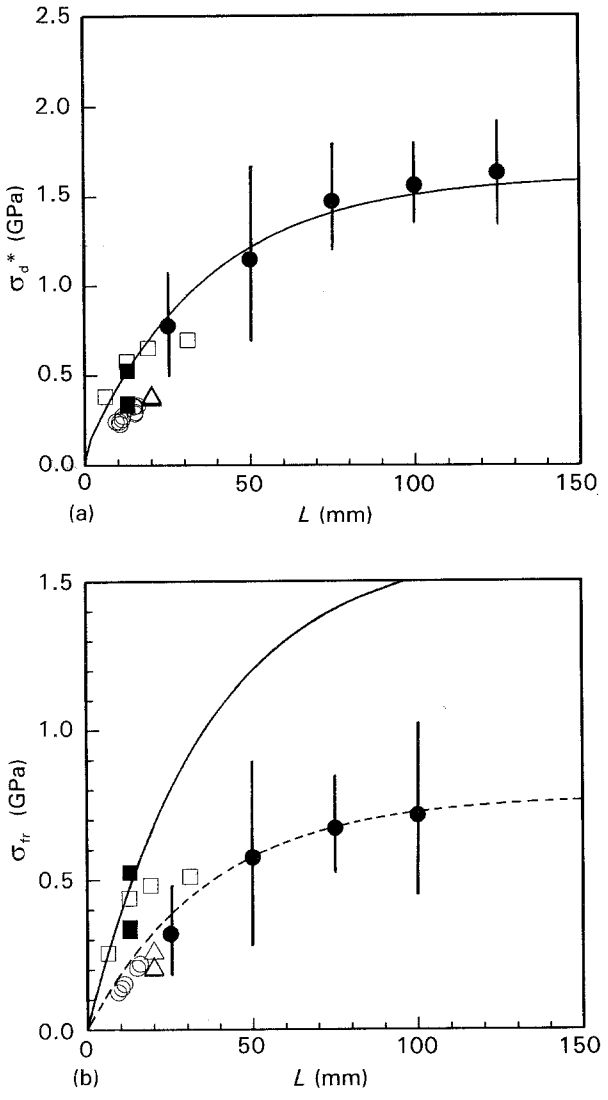

Figure 4 Comparison between experimental results and theoretical predictions of (a) maximum debond stress, σ_d^*, and (b) initial frictional pull-out stress, σ_{fr}, as a function of embedded fibre length, L, for the steel fibre–cement mortar matrix composites. Experimental data taken from (■) Naaman and Shah [6]; (○) Maage [7]; (□) Beaumont and Aleszka [8]; (●) Gray [9]; (△) Mandel *et al.* [10]. Predictions: (——) with residual clamping stress, $q_0 = -50.3$ MPa; (– – –) with corrected $q_0 = -24.2$ MPa.

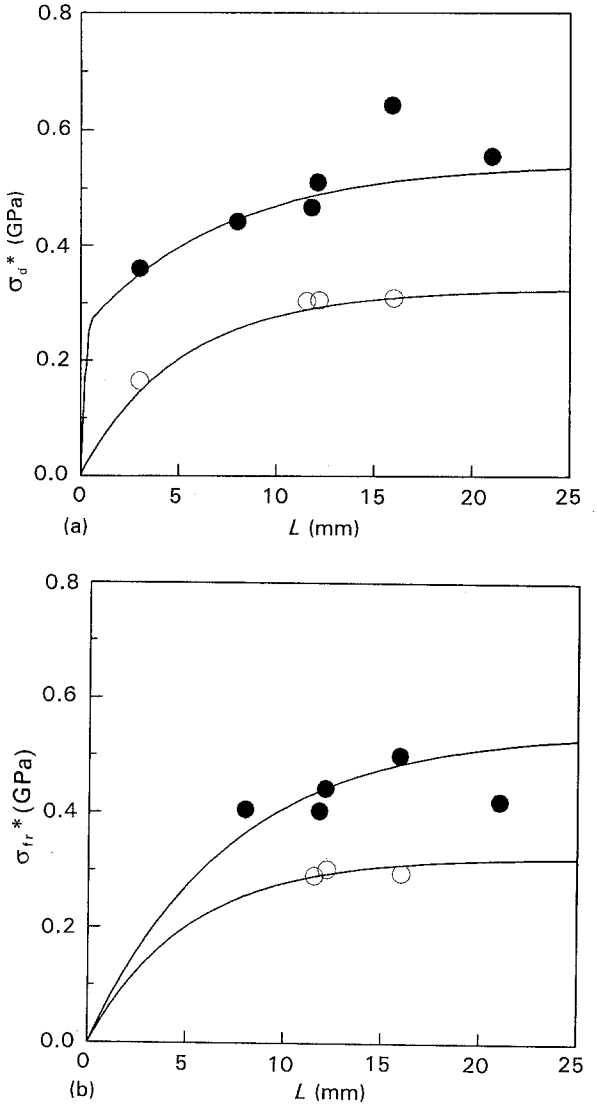

Figure 5 Comparison between experimental results and theoretical predictions of (a) maximum debond stress, σ_d^*, and (b) initial frictional pull-out stress, σ_{fr}, as a function of embedded fibre length, L, for the glass fibre–cement mortar matrix composites. Experimental data taken from Li *et al.* [11]: (○) normal cure in air; (●) accelerated cure in lime-saturated water. (——) Prediction.

The prediction for the maximum debond stress, σ_d^*, agrees well with the experiment over the whole range of embedded fibre length, L, within the experimental data scatter due to different testing methods and materials (Fig. 4a). However, the theory overestimates the initial frictional pull-out stress, σ_{fr}, particularly for long L (Fig. 4b), if the same interfacial parameters are used for prediction. This discrepancy is considered to be a direct result of decay of the frictional bond at the debonded region which effectively reduces the frictional pull-out stresses, σ_{fr}, in the experiment. There are several reasons for the degradation of the frictional resistance: (i) the compaction or densification of cement mortar near the fibre surface [20–22]; (ii) the microcracking and virtual breakdown of the cement mortar at the interface due to the high stiffness and hardness of the fibre relative to the matrix material [20, 21]; (iii) the permanent plastic deformation of the ductile steel fibre after yielding, particularly at a high debond stress for a long embedded fibre; (iv) instantaneous relative slip between the fibre and matrix after the load instability which would slightly reduce the effective embedded fibre length. Among these, the first is the most likely and most influential, which is related to the porous nature of most cement mortar. Bentur *et al.* [23] explained the microstructure of this material in terms of the transition zone which consists of a duplex film of cement, a CH-rich layer, a porous CSH layer and the bulk material in the order from the fibre surface. The weakest region of the transition zone is not necessarily at the actual interface, but is the porous layer as evinced by the low microhardness at a distance approximately 20–40 μm away from the interface [24]. The weak porous layer is densified upon fibre slip after debonding, resulting in enlargement of the matrix hole. Rough steel fibre surface, if any, even on a microscopic scale, may promote the compaction of matrix material.

Therefore, the gross effect turns out to be a significant reduction in the residual clamping stress, q_0 [20,

22] arising from the matrix shrinkage, rather than a reduction in the coefficient of friction, μ. Further, a significant portion of the relaxation of residual clamping stress appears to have occurred at the end of and/or just after the debonding process, as suggested by the progressive load drop (as opposed to the rapid unstable load drop in polymer and ceramic-based composite systems) after the maximum in the pull-out load versus displacement record for this material [9, 10, 22]. Therefore, a correct theoretical prediction is made for the frictional pull-out stress, σ_{fr}, using a lower value of q_0 (reduced from -50.3 MPa to -24.2 MPa) while other parameters are kept constant. The new prediction now gives excellent agreement with experimental results as shown in Fig. 4b. However, it has to be emphasized here that the corrected q_0 value applies only to the point of initial frictional pull-out and there may be further degradation of frictional properties as fibre pull-out continues.

3.3. Glass fibre–cement mortar matrix composites

The glass fibre–cement mortar matrix composite with normal cure displays an even more pronounced stability during the debond process (Fig. 3a) than the steel fibre–cement matrix composites (Fig. 2), as evinced by the predominant (i.e. more than 95%) contribution of the friction stress component to the partial debond stress, σ_d^p, at instability and a very small z_{max} (= 0.14 mm) for an embedded fibre length $L = 25$ mm. Note the negligibly small interfacial fracture toughness, G_{ic} (= 0.03J m^{-2}), and the corresponding σ_0 (= 0.01 GPa) for this composite system compared with those of steel fibre–cement matrix interface in Table III. Accelerated cure of the composite in a lime-saturated water at an elevated temperature significantly increases the interfacial properties (e.g. almost three orders of magnitude for G_{ic}, in particular). This consequently increases the contribution of crack-tip debond stress, σ_ℓ, to the partial debond stress, σ_d^p, outdoing that of the friction stress component over almost the whole debond process (Fig. 3b). However, as the crack tip approaches the embedded fibre end at the end of debonding, the crack-tip debond stress, σ_ℓ, decreases towards zero while the frictional stress component increases rapidly. Eventually, at instability where the maximum debond stress, σ_d^*, is obtained, these two stress components contribute roughly 50% each of the total for an embedded fibre length, $L = 25$ mm. This is followed by a small stress drop to a new value corresponding to the initial frictional pull-out stress, σ_{fr}. z_{max} is only marginally increased in real terms (i.e. from 0.14 mm to 0.64 mm) due to the accelerated cure, which is even smaller than the composite system containing steel fibres. On the whole, an accelerated cure does not much impair the stability of the debond process in this composite although substantial changes in the nature and quality of the interfacial bond are noted.

For glass fibre–cement mortar matrix composites at the early stage of curing in the absence of substantial hydration of the cement, the bond at the fibre–matrix interface is predominantly mechanical in nature [15]. In addition, because there is a number of pores present in the matrix material, gathering near the interface in particular, the interfacial bond strength may not be substantial. This is verified by the very small interfacial fracture toughness ($G_{ic} = 0.03$ J m^{-2}, Table III) for the composites with 3 day normal cure in air. With age, the CH layer forming at the interface when cement is hydrated becomes progressively more crystalline and less porous. Therefore, after a substantial period of cure, as for the composites with accelerated cure in a lime-saturated water bath at an elevated temperature, the composite can be considered as being completely mature and the interphase as being almost completely in solid contact between the fibre and the CH crystals in the matrix. (For example, according to the time–temperature equivalence procedure, 1 day of wet storage at 50 °C corresponds approximately to 100 days in water at 10 °C [11].) The resulting interfacial bond becomes stronger not only as a result of chemical reaction but also due to the increased effective fibre–matrix contact area at the interface associated with densification of the matrix material [25]. Thus, the interfacial fracture toughness, G_{ic} (which is a measure of chemical bond at the interface), is increased by almost three orders of magnitude (i.e. from 0.03 J m^{-2} to 22.82 J m^{-2}). There are also some changes in the residual clamping stress, q_0 (65% increase) and the coefficient of friction, μ (40% reduction) with an overall increase in the maximum frictional shear strength, $\tau_{f(max)}$($\approx -\mu q_0$) by about 20%. Clearly the improvement in the overall frictional bonding is attributed to the increase in the apparent contact area actually involved in frictional sliding at the debonded interface. However, it appears that the significantly lower Young's modulus and even smaller effective radius of the glass fibre (compared to the steel fibre) do not cause any appreciable degradation of interfacial properties during or after complete debonding. The predictions for the maximum debond stress, σ_d^*, and initial frictional pull-out stress, σ_{fr}, after complete debonding agree reasonably well with experiments over the range of embedded fibre length, L, studied (Fig. 5a and b), though only a limited number of data points are available. This result is considered to be remarkable, despite the uncertainties and approximations of the actual values for elastic properties and radii of the constituents used for the calculations.

4. Discussion

It has been postulated in Section 3.2 that the degradation of interfacial properties during frictional pull-out of rigid steel fibres from cement mortar matrix is responsible for the significant discrepancy between experiments and theoretical prediction, if the same interfacial properties were used for prediction of both the maximum debond stress, σ_d^*, and post-debond frictional pull-out stress, σ_{fr}. Because of this anomaly, early attempts used two completely different approaches to fit the data for σ_d^* and σ_{fr} separately. For example, Beaumont and Aleszka [8] determined the interfacial shear bond strength, τ_b, in a curve-fitting

technique using early models developed based on a shear strength criterion including Greszczuk [26] and Takaku and Arridge [27], in which the effect of friction at the debonded region is not properly taken into account so that unstable debonding is assumed, regardless of the embedded fibre length, L, and the nature of the bond at the fibre–matrix interface. They estimated q_0 and μ using an expression similar to the simplified form of Equation 2. Therefore, no correlation has been established between these two stresses σ_d^* and σ_{fr}. Later, Gray [9] followed a similar procedure and added several other models including Lawrence [28], Bartos [29] and Laws [30] to estimate the interfacial properties. These models considered the friction but neglected completely the Poisson contraction of the fibre subjected to tension, so that the interfacial friction shear stress is constant along the debonded fibre length. As a result, and even worsened by the microstructural anomaly observed in the present study, these models inevitably gave the interfacial shear bond strength, τ_b, overestimated by more than an order of magnitude compared to those estimated based on an earlier model [26, 27] (e.g. τ_b = 3.1–3.3 MPa to 38.4–94.7 MPa). It has been shown in Part I of this paper [3] that a simplified assumption of constant frictional shear stress results in a significant overestimate of the friction stress component of the partial debond stress, σ_d^p, during the debond process and thus the maximum debond stress, σ_d^*, for a given embedded fibre length, L, leading to a premature debonding instability. It is only in recent years that the degradation of interfacial properties in steel fibre–cement matrix composites has been recognized and taken into account for a correct analytical model of fibre pull-out. Naaman *et al.* [22, 31] assumed an exponential decay of the residual clamping stress, q_0, during frictional pull-out after complete debonding, showing good agreement in the pull-out force versus slip displacement relationship between prediction and experiments.

It is interesting to note that there are similarities, as well as differences, between the resultant property changes due to two different sources of microstructural change as discussed in Section 3. Compaction or densification of cement mortar matrix, regardless of whether it is limited in the interphase region or it occurs in bulk, certainly increases the stiffness (or Young's modulus) of the matrix material. However, at the same time, it also increases or decreases the effective radius of the matrix hole, depending on the source of the microstructural change which determine the direction of compaction relative to the fibre surface: i.e. frictional sliding of rigid fibres against the porous matrix wall for steel fibre–cement matrix composites or hardening of matrix material towards the fibre surface due to ageing as for the glass fibre–cement matrix composites. For the former system these two property changes balance each other reducing their individual effectiveness, while for the latter system they produce synergic effects. Without knowledge of the exact variation of Young's modulus or effective radius of the matrix hole, it is reasonable to regard the gross effect as a change in interfacial properties.

Because even a small difference in fibre surface condition, matrix composition, composite cure condition, and testing configuration including single or multiple fibres, specimen geometry and loading method may influence the pull-out results, it is difficult to compare the estimated value of interfacial properties obtained in the present study with those previously predicted for similar fibre–matrix system. It is worth noting, however, that the properties determined in this study for the steel fibre–cement matrix composites (i.e. $G_{ic} = 2.5\ J\,m^{-2}$, $q_0 = -24.2$ MPa and $\mu = 0.082$ and $\tau_{fr} = 1.95$ MPa) compare most favourably with some selected values reported in the literature (e.g. $q_0 = -24.6$ MPa, $\mu = 0.09$ [9]; τ_{fr} = 1.4–1.8 MPa [22]; $G_{ic} = 2.41$–$2.53\ J\,m^{-2}$, τ_{fr} = 1.3 MPa [32]). In fact, in view of the variables and discontinuous nature of the interfacial bond at the microstructural level in cement matrix composites [9], unlike more homogeneous matrices including polymers, these interfacial properties as a whole may represent only the actual average values along the whole interface rather than apparent material constants.

5. Conclusion

Using an improved theoretical analysis developed in Part II of this paper interfacial properties have been characterized with regard to the debond and frictional pull-out stresses in cement mortar matrix composites reinforced with steel fibres and glass fibres. The interfacial properties, including the interfacial fracture toughness, G_{ic}, residual clamping stress, q_0, and the coefficient of friction, μ, are determined in a procedure suggested in Part I of this paper.

It is shown from the plots of partial debond stress, σ_d^p, versus debond length, ℓ, that these composites are typical of principally mechanical bonding at the interface, as evinced by the very small z_{max} (which is a measure of the maximum bond length for unstable debonding) even for those cured in an accelerated condition. The stability of the interfacial property-dependent debond process in these cement matrix composites is also reflected sensibly by the negligible amount of stress (or load) drop after the maximum (i.e. from the maximum debond stress, σ_d^*, to a lower value corresponding to the initial, frictional pull-out stress, σ_{fr}).

It is identified that the gross effect of densification or compaction of cement mortar matrix is different in these composites containing two different reinforcing fibres due to completely different causes of the microstructural change: densification of cement matrix during or after complete debonding degrades the interfacial properties, residual clamping stress, q_0, in particular, for those with steel fibres; whereas densification and associated crystallization of cement matrix around the fibre occurring in accelerated cure improve the interfacial properties, both chemical and mechanical, for those with glass fibres.

For the steel fibre–cement mortar matrix composites, the maximum debond stress, σ_d^*, prediction agrees well with the experimental result over the whole range of embedded fibre length, L, studied.

However, the theory overestimates the post-debond frictional pull-out stress, σ_{fr}, particularly for long L, if the same interfacial properties are used for prediction. This discrepancy is presumably a direct result of gradual degradation of the frictional bond at the interface due mainly to compaction of the porous cement mortar surrounding the fibre after interfacial debonding. This effectively reduces the residual clamping stress, q_0, arising from shrinkage of the cement matrix. Therefore, a correct theoretical prediction is made for the initial frictional pull-out stress, σ_{fr}, after complete debonding using a lower value of q_0 while other properties are kept constant, which gives good agreement with experimental results.

For glass fibre–cement mortar matrix composites, a cure in a lime-saturated water bath accelerates hydration of cement, eliminating pores and thus densifying the cement matrix. This results in a significant improvement in the interfacial bond quality due to the formation of CH crystals and an apparent increase in the actual contact area between the fibre and matrix. It is noted that the interfacial fracture toughness, G_{ic}, is increased by almost three orders of magnitude while the maximum frictional bond strength, $\tau_{f(max)}(\approx -\mu q_0)$, is increased by about 20%.

Therefore, following the successful application of the improved fibre pull-out model to several epoxy and ceramic matrix composites in Part II of this paper, it is demonstrated here in Part III that the model, in general, can be applied to characterize the interfacial properties of brittle fibre–brittle matrix composites, regardless of the nature of bond at the interface.

Acknowledgements

The authors thank the Australian Research Council (ARC) for the continuing support of this work. L.M.Z. was supported by a University of Sydney Postgraduate Research Scholarship and a Junior Research Fellowship, and J.K.K. by an Australian Postdoctoral Research Fellowship awarded by the ARC. Part of the paper was presented at FRAMCoS-1, Breckenridge, CO, USA, June 1992.

References

1. J. K. KIM and Y. W. MAI, in "Structure and Properties of Fibre Composites", Vol. 13, edited by T. W. Chou, (VCH, Weinheim, Germany, 1992) Ch 6, in press.
2. L. M. ZHOU, J. K. KIM and Y. W. MAI, *J. Mater. Sci.* **27** (1992), 3155.
3. J. K. KIM, C. BAILLIE and Y. W. MAI, *ibid.* **27** (1992) 3143.
4. L. M. ZHOU, J. K. KIM and Y. W. MAI, *Comps. Sci. Technol.* **45** (1992) 153.
5. J. K. KIM, C. BAILLIE and Y. W. MAI, *Scripta Metall. Mater.* **25** (1991) 315.
6. A. E. NAAMAN and S. P. SHAH, *ASCE J. Struct. Div.* **102** (1976) 1537.
7. M. MAAGE, *Mater. Struct.* **10** (1977) 297.
8. P. W. R. BEAUMONT and J. C. ALESZKA, *J. Mater. Sci.* **13** (1978) 1749.
9. R. Y. GRAY, *ibid.* **19** (1984) 1680.
10. J. A. MANDEL, S. WEI and S. SAID, *ACI Mater. J.* **12** (1987) 101.
11. Z. LI, B. MOBASHER and S. P. SHAH, *J. Amer. Ceram. Soc.* **74** (1991) 2156.
12. P. BARTOS, *Int. J. Cement Compos.* **3** (1981) 159.
13. B. A. PROCTOR, D. R. OAKLEY and K. C. LITHERLAND, *Composites* **13** (1982) 173.
14. R. C. DE VEKEY and A. J. MAJUMDAR, *Mag. Concr. Res.* **20** (1968) 229.
15. *Idem, J. Mater. Sci.* **5** (1970) 183.
16. V. LAWS, A. A. LANGLEY and J. M. WEST, *ibid.* **21** (1986) 289.
17. V. M. KARBHARI and D. J. WILKINS, *ibid.* **26** (1991) 5888.
18. C. H. HSUEH, *Mater. Sci. Engng* **A123** (1990) 1.
19. *Idem. ibid.* **A123** (1990) 67.
20. D. J. PINCHIN and D. TABOR, *Cement Concr. Res.* **8** (1978) 139.
21. Y. WANG, V. C. LI and S. BACKER, *Int. J. Cem. Compos. Lightwt. Concr.* **10** (1988) 143.
22. A. E. NAAMAN, G. G. NARMUR, J. M. ALWIN and H. S. NAJM, *ASCE, J. Struct. Engng* **119** (1991) 2769.
23. A. BENTUR, S. DIAMOND and S. MINDESS, *J. Mater. Sci.* **20** (1985) 3610.
24. S. WEI, J. A. MANDEL and S. SAID, *J. Amer. Concr. Inst.* **83** (1986) 597.
25. M. S. STUCKE and A. J. MAJUMDAR, *J. Mater. Sci.* **11** (1976) 1019.
26. L. B. GRESZCZUK, in "Interface in Composites", ASTM STP 452 (American Society for Testing and Materials, Philadelphia, PA, 1969) pp. 42–58.
27. A. TAKAKU and R. G. C. ARRIDGE, *J. Phys. D. Appl. Phys.* **6** (1973) 2038.
28. P. LAWRENCE, *J. Mater. Sci.* **7** (1972) 1.
29. P. BARTOS, *ibid.* **15** (1980) 3122.
30. V. LAWS, *Composites* **13** (1982) 145.
31. A. E. NAAMAN, G. G. NARMUR, J. M. ALWAN and H. S. NAJM, *ASCE J. Struct. Engng* **119** (1991) 2791.
32. J. K. MORRISON, S. P. SHAH and Y. S. JENQ, *ASCE. J. Engng Mech.* **114** (1988) 277.

Received 22 July 1992
and accepted 4 January 1993